UC Berkeley

Title

Phonon Polariton-assisted Infrared Nanoimaging of Local Strain in Hexagonal Boron Nitride

Permalink

https://escholarship.org/uc/item/2x99p178

Journal

ISSN

Authors

Lyu, Bosai
Li, Hongyuan
Jiang, Lili
et al.

Publication Date

DOI

Phonon polariton assisted infrared nano-imaging of local strain in hexagonal boron nitride

Bosai Lyu[1,2], Hongyuan Li[1,2], Lili Jiang[3], Wanfei Shan[1,2], Cheng Hu[1,2], Aolin Deng[1,2], Zhe Ying[1,2], Lele Wang[1,2], Yiran Zhang[1,2], Hans A. Bechtel[4], Michael C. Martin[4], Takashi Taniguchi[5], Kenji Watanabe[5], Weidong Luo[1,2,6], Feng Wang[3,7,8], Zhiwen Shi[1,2]*

[1]Key Laboratory of Artificial Structures and Quantum Control (Ministry of Education), School of Physics and Astronomy, Shanghai Jiao Tong University, Shanghai 200240, China.

[2]Collaborative Innovation Center of Advanced Microstructures, Nanjing 210093, China.

[3]Department of Physics, University of California at Berkeley, Berkeley, CA, USA.

[4]Advanced Light Source Division, Lawrence Berkeley National Laboratory, Berkeley, CA, USA.

[5]National Institute for Materials Science, 1-1 Namiki, Tsukuba, 305-0044, Japan.

[6]Institute of Natural Sciences, Shanghai Jiao Tong University, Shanghai 200240, China.

[7]Materials Science Division, Lawrence Berkeley National Laboratory, Berkeley, CA, USA.

[8]Kavli Energy NanoSciences Institute at the University of California, Berkeley and the Lawrence Berkeley National Laboratory, Berkeley, CA, USA.

*To whom correspondence should be addressed. Email: zwshi@sjtu.edu.cn

KEYWORDS: Local strain, 2D materials, infrared nanoscopy, phonon polaritons

ABSTRACT:

Strain plays an important role in condensed matter physics and materials science because it can strongly modify the mechanical, electrical, and optical properties of a material, and even induce a structural phase transition. Strain effects are especially interesting in atomically thin two-dimensional (2D) materials, where unusually large strain can be achieved without breaking them. Measuring the strain distribution in 2D materials at the nanometer scale is therefore greatly important but is extremely challenging experimentally. Here, we use near-field infrared nanoscopy to demonstrate phonon polariton assisted mapping and quantitative analysis of strain in atomically thin polar crystals of hexagonal boron nitride (hBN) at the nanoscale. A local strain as low as 0.01% can be detected using this method with ~ 20 nm spatial resolution. Such ultra-sensitive nanoscale strain imaging and analysis technique opens up opportunities for exploring unique local strain structures and strain-related physics in 2D materials. In addition, experimental evidence for local strain induced phonon polariton reflection is also provided, which offers a new approach to manipulate light at deep sub-wavelength scales for nano-photonic devices.

TEXT:

Two-dimensional (2D) materials have rich intrinsic properties with a large flexibility to build heterostructures, and thus offer a fascinating platform for exploring fundamental physics and device applications. Hexagonal boron nitride (hBN) crystals have recently attracted much research interest. As an atomically flat insulating material, it provides an ideal substrate for functional van der Waals heterostructures,[1-3] and enabled the discovery of novel 2D superlattice phenomena,[4-7] such as Hofstadter's butterfly[4,8] and strongly correlated Mott insulating states[5]. In addition, hBN itself hosts tunable low-loss phonon polariton modes with strongly compressed polariton wavelengths,[9-10] which makes it a promising material for future nano-photonic devices and circuits.

Strain provides an extra degree of freedom to modify the intrinsic properties of a material and can even induce a structural phase transition. Strain effects are more remarkable in atomically thin 2D materials, where large strain can be achieved without breaking the material. Various strain-induced phenomena in 2D materials, including modulation of electronic structure,[11-12] generation of a pseudo-magnetic field,[11,13] topological valley transport,[14] soliton-dependent plasmon reflection,[15] reduction of the direct bandgap and exciton funneling[16], and structural phase transitions,[17] have been investigated. Consequently, obtaining the nanoscale strain distribution in 2D materials is crucial to fully understand strain-induced phenomena. However, in-situ mapping of local strain in 2D materials with nanometer spatial resolution and high sensitivity has been an outstanding challenge.

Classical methods like X-ray diffraction (XRD)[18] and neutron scattering[19] offer high sensitive measurement of strain, but they usually require bulk samples and their spatial resolution is poor. Transmission electron microscopy provides lattice scale imaging of local strain but requires sample thinning process, which may change the original strain field.[20] Conventional far-field optical techniques, such as Raman spectroscopy,[16] provide in-situ and noninvasive characterization of strain field but diffraction typically limits the spatial resolution to the micrometer scale. Near-field optical techniques allow high spatial resolution imaging beyond the diffraction limit. One approach is tip-enhanced Raman spectroscopy (TERS), which can measure phonon frequency with nanometer spatial resolution.[21-22] However, because Raman scattering is an inelastic light scattering process, TERS signals of 2D materials tend to be very weak, usually requiring samples to be placed on metal substrates, such that in-situ and on-chip strain detection is extremely difficult. Another possible near-field approach for nanoscale strain mapping is infrared (IR) scanning near-field optical microscopy (s-SNOM), which relies on elastic scattering of the incident infrared radiation. As a result, infrared s-SNOM can provide much stronger signals and better signal-to-noise ratios than TERS. Previous studies have shown that infrared s-SNOM provides a powerful tool for probing propagating plasmons and phonon polaritons.[9-10, 14-15, 23-26] Detection of local strain using infrared s-SNOM has also been demonstrated at the surface of 3D bulk materials.[27-30] However, due to the entanglement of strain in different orientations of 3D crystals, it is difficult to analytically solve their local strain structures. A quantitative comparison between the near-field infrared measurement and

theoretical calculation has not been realized yet. Therefore, the near-field infrared nano-imaging of local strain remains semi-quantitative and its analysis is ambiguous.

In this paper, we demonstrate high-sensitive nano-imaging and quantitative analysis of an analytic local strain field in atomically thin 2D hBN crystals with infrared s-SNOM. We find that, in addition to local dielectric function, the phonon polaritons can dominate the near-field infrared profile in at certain frequencies in the local strain region, where phonon polariton reflection and interference occur. Furthermore, the strain induced shifts of phonon frequencies are directly measured with the assistance of a broadband synchrotron light source, and calculated using first-principles density functional theory (DFT) combined with an analytic model. The sensitivity of the near-field infrared method in detecting strain in hBN crystals is estimated to be 10^{-4}. Such ultra-sensitive nanoscale strain mapping technique opens up opportunities for exploring unique local strain structures and strain-related phenomena in 2D materials. In addition, the observed phonon polariton reflection induced by the local strain offers a new approach to manipulate light at deep sub-wavelength scales for nanophotonic devices.
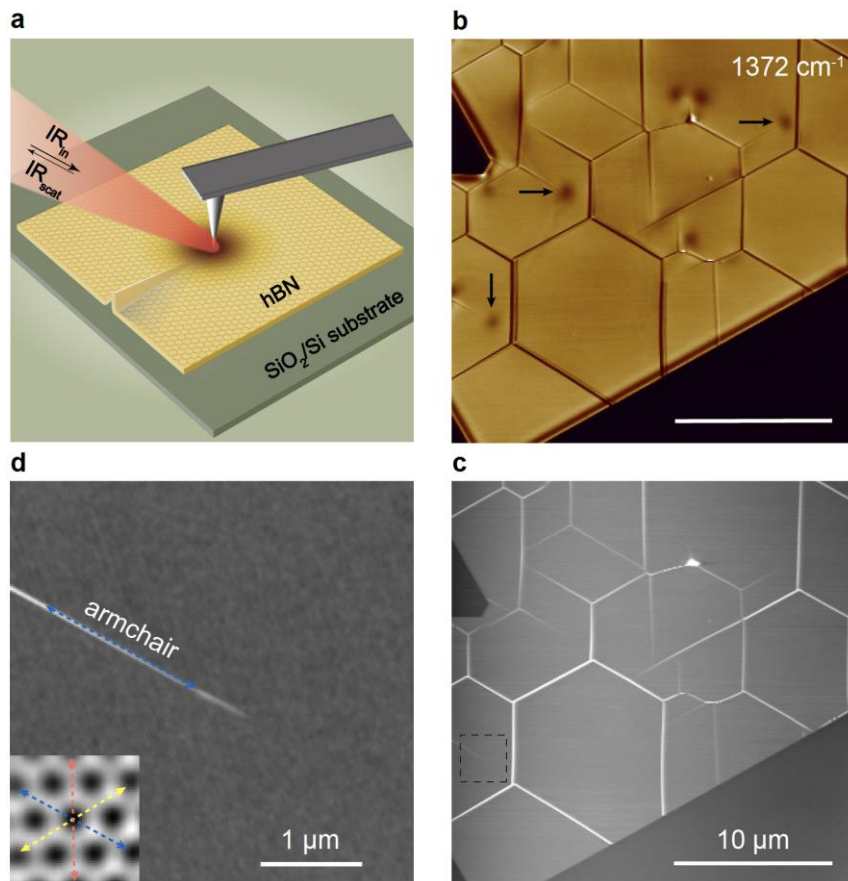
Figure 1. Mapping of local strain in hBN through infrared nano-imaging. (a) Illustration of the near-field infrared (IR) measurement of local strain in hBN. Infrared light was focused on the apex of a conductive AFM tip, and the back-scattered light was collected by an MCT detector in the far field. (b) The near-field IR image of a typical annealed hBN flake (~ 6 nm thick) with wrinkles on a SiO$_2$/Si substrate, taken at a frequency of 1372 cm^{-1}, shows prominent dark spots near wrinkle ends (denoted by black arrows). (c) The corresponding AFM topography image of the hBN flake in (b). (d) A close-up AFM topography image of the wrinkle in the dashed square in (c) The inset shows a lattice-resolution AFM image of a small area of hBN aside the wrinkle, which reveals that the wrinkle is right along the armchair direction. Three armchair directions of the hBN crystal are denoted by blue, yellow and red dashed arrows.

Thin hBN flakes were mechanically exfoliated onto SiO_2/Si substrate from a bulk hBN crystal. Wrinkles were generated in hBN flakes after an annealing process (see Supporting Information Section 1 for details), due to a mismatch in the thermal expansion coefficient between hBN (negative) and the silicon substrate (positive). Theoretically, in the region near the end of a wrinkle, there should exist an in-plane local compressive strain due to the discontinuity in the interior angle of the hBN flake. At the end of the wrinkle, the interior angle is less than 2π, which makes the region near the end of a wrinkle a topological vertex. Such a vertex leads to in-plane local strain in the hBN flake (Supporting Information Section 2).

An infrared s-SNOM was employed to probe the local strain in annealed hBN samples, the schematic of which is shown in Figure 1a. In brief, an infrared laser beam was focused onto the apex of a conductive atomic force microscope (AFM) tip. Back-scattered light from the tip apex was collected and measured by a MCT detector placed in the far field (see Methods for details). The tip-enhanced infrared scattering provides a local probe of the material infrared responses with ~ 20 nm spatial resolution. Figure 1b and 1c present near-field IR and topography images of a 6-nm-thick hBN flake. The IR image is taken at a selected excitation frequency of 1372 cm^{-1}, which is the frequency of the in-plane transverse optical (TO) phonon of our annealed hBN sample[10]. In both images, network of wrinkles with intersection angles of either 60° or 120° were observed, which implies that they are all aligned along certain crystal direction. A high-resolution friction image shown in the inset of Figure 1d uncovers the crystallographic orientation of the hBN flake and reveals that all wrinkles are along the armchair

direction, which is probably due to the lower formation energy along the armchair direction and agrees with previous experimental observations[31]. In addition to those wrinkles, prominent dark spots are observed near the end of the wrinkles in the IR image, whereas no corresponding features can be discerned in the topography image. A close-up topography image (Figure 1d) of the wrinkle in the dashed square in Figure 1c further confirms that the hBN sample is perfectly flat near the wrinkle end without any feature. The observed IR contrast reflects a change in the local dielectric constant of hBN, which is presumably induced by the local strain near the end of a wrinkle. Any strain will change the chemical bond length of hBN, shift its resonating phonon frequency, alter the dielectric constant, and modify the near-field optical response. More specifically, a compressive strain will shift the hBN phonon to higher frequency, and decrease the IR response at frequencies below the resonating phonon frequency, as shown in Figure 2a.

To systematically study the local strain in hBN, we collected near-field IR images of a strained area with a spectral range from 1340 cm^{-1} to 1410 cm^{-1}, as shown in Figure 2b to 2i. The strained area always features a dark spot at frequencies below 1372 cm^{-1}, and gradually evolves into a bright spot in higher frequency range. As 1372 cm^{-1} corresponds to the in-plane TO phonon of hBN, for frequencies above 1372 cm^{-1}, there exist propagating phonon polariton modes in hBN flakes. Such nonlocal polariton modes would contribute to and further modify the near-field IR signal.[9-10] Therefore, we divided the experimental data into two groups: one at frequencies below 1372 cm^{-1} (with no polariton modes) and the other at frequencies above 1372 cm^{-1} (with polariton

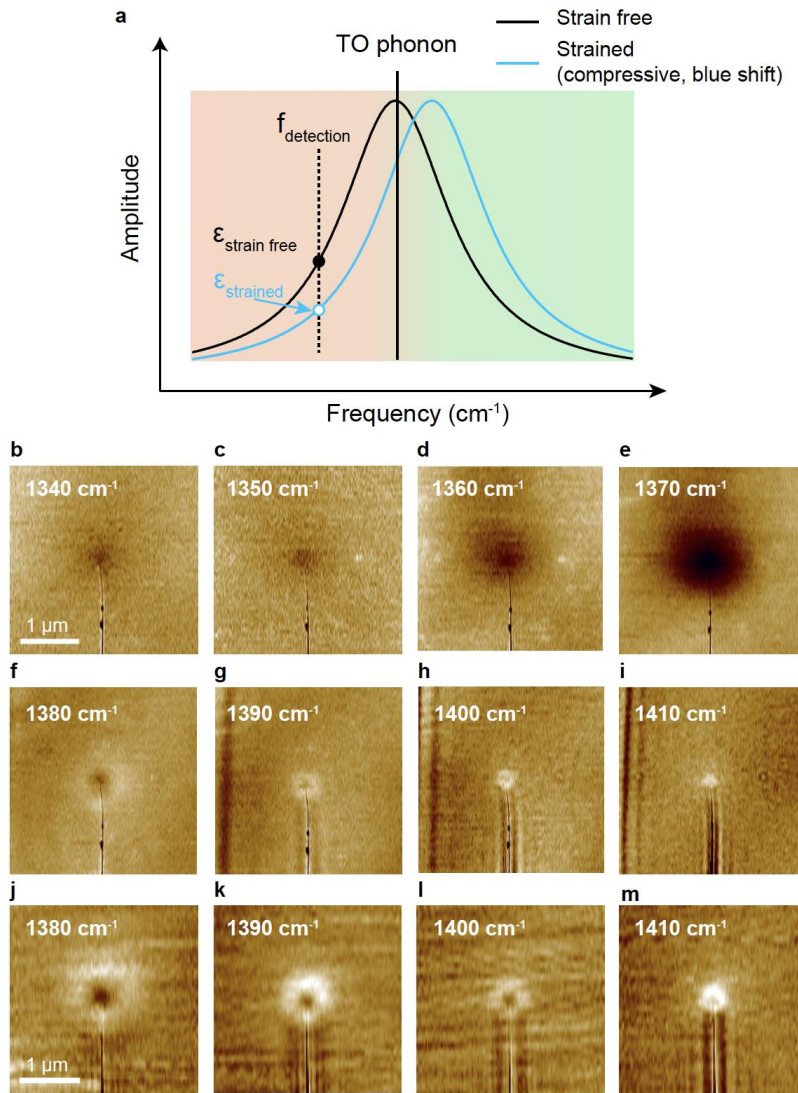modes), and discuss them respectively in detail below.

Figure 2. Frequency-dependent near-field IR response of the local strain. (a) Illustration of compressive strain induced phonon frequency shift and near-field IR contrast. The black and blue curves represent the absolute value of the dielectric function of strain-free and compressive-strained hBN, respectively. (b)-(i) Near-field IR images of local strain area in a 5-nm-thick hBN sample at different excitation frequencies. In (b)-(e), at frequencies lower than TO phonon, near-field IR

images feature simply a dark spot at the strained area. In (f)-(i), at frequencies higher than TO phonon, phonon polariton starts to emerge and its interference modifies the near-field IR images. (j)-(m), Infrared images of local strain in a thicker (~10 nm) sample with smaller strain; they show a greater feature size than the upper panels at the same frequencies, indicating that the near-field signal at frequencies higher than 1372 cm^{-1} is dominated by nonlocal phonon polaritons. Scale bar: 1 μm.

We first investigate the near-field IR images of the strained area at frequencies below the TO phonon, as displayed in Figure 2b to 2e. As there are no propagating phonon polaritons in this frequency range, the near-field optical signal is simply determined by the local dielectric function of hBN underneath the tip apex. Due to the existence of compressive strain around the end of the wrinkle, the hBN phonon resonance shifts to a frequency higher than 1372 cm^{-1}, as illustrated in Figure 2a. Consequently, the absolute value of the dielectric function for the strained area is smaller than that for the unstrained area in the frequency range below 1372 cm^{-1}, which leads to a lower IR response and dark spots in the strained area, as shown in Figure 2b-2e. More quantitatively, the difference in dielectric function has a maximum around the resonating frequency of 1372 cm^{-1} and diminishes far away from the resonating frequency. Consequently, the observed dark spot is most prominent at 1372 cm^{-1}, and gradually blurs for frequencies further away.

At frequencies higher than 1372 cm^{-1}, the near-field IR images exhibit distinct and rich features, owing to the existence of propagating nonlocal phonon polaritons. It shows a dark spot in the center area and a bright ring outside at 1380 cm^{-1}, and gradually evolves to a bright spot with increasing excitation frequency, as shown in Figure 2f-2i.

Such an intriguing IR response may come from either the local dielectric function, or propagating nonlocal phonon polaritons, or both of them. To find out the main origin, we collected data from two different hBN samples at identical experimental conditions. The first sample (Figure 2f-2i) is thinner (~5 nm) with a larger strain, whereas the second sample (Figure 2j-2m) is thicker (~10 nm) with a smaller strain (see Supporting Information Section 2 for the estimation of the strain magnitude). The phonon polariton of hBN has a hyperbolic dispersion relation and consequently has a linearly wavelength dependence on sample thickness.[9-10] Therefore, if the observed near-field feature is strongly affected by phonon polaritons, its characteristic size will scale with phonon polariton wavelength and thus sample thickness. Otherwise, the size of the feature will increase with increasing strain. From the experimental IR images of Figure 2e-2m, we note that the lower panels from the sample with larger thickness and smaller strain show a greater feature size, which indicates that the near-field signal is strongly affected by nonlocal phonon polaritons. The phonon polariton induced modulation of IR response can be understood in the following way. When scanning an hBN sample with s-SNOM, phonon polaritons are excited by the nano-tip and propagate in the hBN flake. They get partially reflected at the strained region where the dielectric constant exhibits a gradient and the polariton wavelength experiences a change. The reflected phonon polaritons will modify the scattered near-field signal at the tip position and induce optical contrast in the near-field IR images (see Supporting Information Section 3 for more experimental evidence).
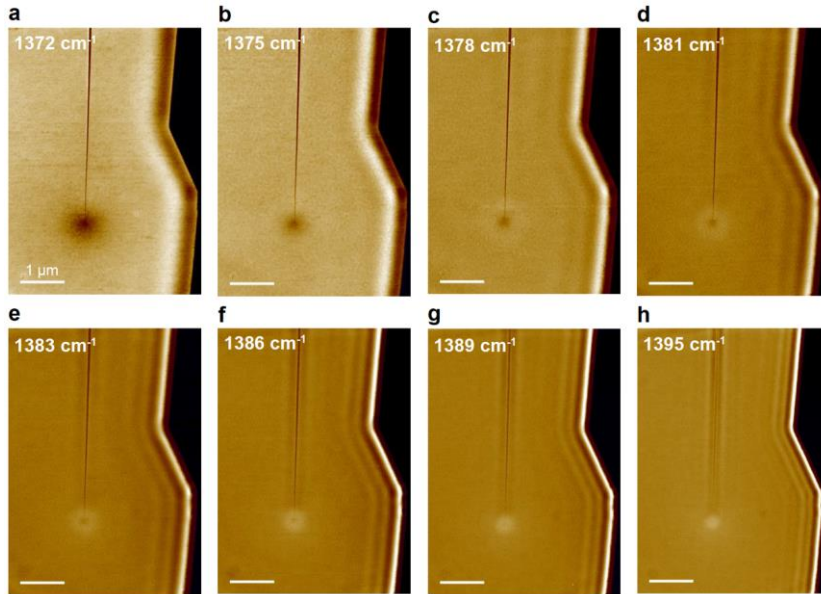
Figure 3. Comparison of near-field IR response between a local strain area and a natural edge of hBN. It is noted that phonon polariton interference around areas of local strain are similar to those around the edge. Both show dark features at 1372 cm^{-1}, and gradually change with increasing illuminating laser frequency until they evolve into bright features at 1395 cm^{-1}. In addition, as the polariton wavelength near the sample edge progressively gets shorter from 1372 cm^{-1} to 1395 cm^{-1}, so does the characteristic length of the feature around the local strain area. Scale bar: 1 μm.

To further confirm that the near-field IR response at frequencies higher than 1372 cm^{-1} is strongly affected by nonlocal propagating polaritons, we collected data from a sample that includes both a strain area and a natural edge and compare their near-field IR features. A series of infrared images taken at frequencies from 1372 cm^{-1} to 1395 cm^{-1} are presented in Figure 3. Near-field IR signals around the local strain area are similar to those around the edge. Both show dark features at 1372 cm^{-1}, and change gradually with increasing illuminating laser frequency, and finally evolve into a bright

feature at 1395 cm^{-1}. In addition, while the polariton wavelength near the sample edge progressively gets shorter from 1372 cm^{-1} to 1395 cm^{-1}, the characteristic length of the local strain area also decreases, showing the same trend. Such similarity in the IR features and their evolution behavior over a broad frequency range confirm that the IR response of the strained area is affected by nonlocal phonon polaritons.

A quantitative phonon frequency shift in the local strain area is measured using broadband synchrotron infrared nanospectroscopy (SINS, see Methods).[10, 32] With a broadband synchrotron IR light source that covers the whole range of the hBN phonon band and detection by interferometric heterodyne amplification, one can directly measure the shifted phonon frequency of the strained area from the IR spectra. As illustrated in Figure 4a, we performed a line scan from the center of strain area (blue dot) to unstrained area (pink dot). Eight nano-Fourier transform infrared (nano-FTIR) spectra were collected along the white dashed arrow and plotted in Figure 4b. Each spectrum features a peak around 1372 cm^{-1} but with slightly shifted frequency. Peak positions are extracted through Lorentz fitting. A gradual shift of peak position from 1372 cm^{-1} to 1374 cm^{-1} can be seen from the spectra and a frequency shift of ~ 2 cm^{-1} is observed at the center of the strained region.
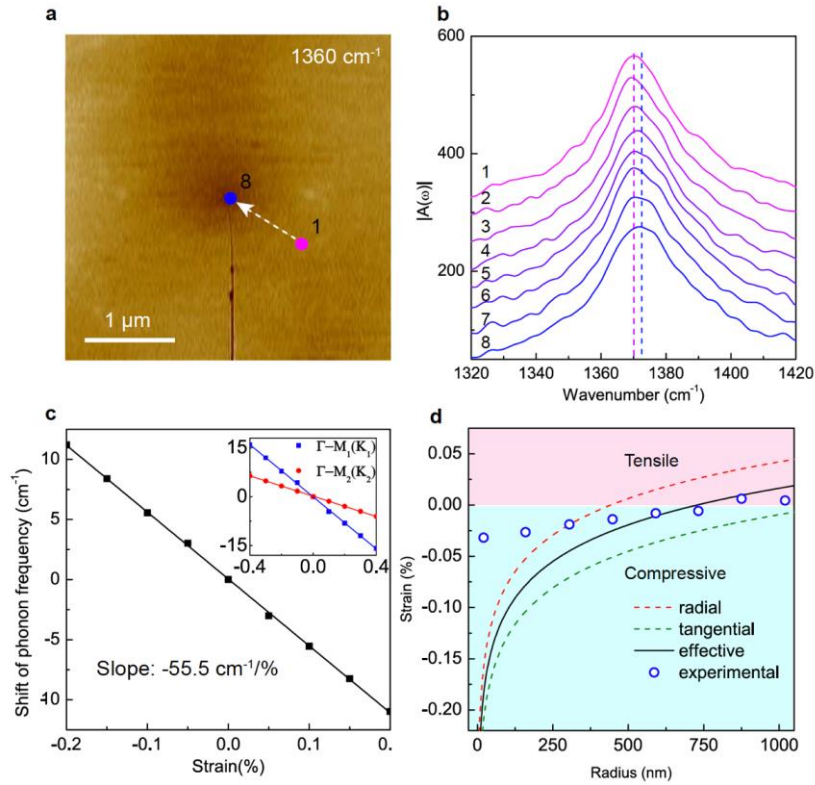
Figure 4. Quantitative analysis of the local strain. (a) near-field IR image of the 5-nm-thick hBN sample shown in Figure 2(b)-(i). The excitation frequency is 1360 cm^{-1}. (b) Nano-FTIR spectra collected along a line scan shown in (a). A gradual frequency shift is observed. (c) First-principles calculation results for hBN TO phonon frequency shift under a isotropic biaxial strain. Inset: the splitting of TO phonon mode by an anisotropic uniaxial strain due to the symmetry breaking. (d) Theoretical results of local strain distribution in radial (red dashed curve) and tangential (green dashed curve) directions, and the averaged effective strain (black curve) for the sample in (a). Experimental strain distribution (blue circles) are obtained from Lorentz fitting of phonon frequency shift in IR spectra in (b) combined with first-principles calculation results in (c).

In order to acquire strain magnitude from the shifted phonon frequency, a quantitative relation of strain and phonon frequency shift is required. First-principles

density functional theory (DFT) calculations within the local-density approximation (LDA) were conducted to calculate the frequency of hBN TO phonon mode under strain (see Supporting Information Section 4 for details). The main calculated results can be summed up in two points. First, the TO phonon resonance frequency will shift linearly by a slope of -55.5 cm^{-1}/% with a uniform in-plane strain applied (Figure 4c). Second, if the in-plane strain is anisotropic, the TO phonon at Γ point would split into two due to the symmetry breaking (inset of Figure 4c). Taking the high symmetric directions $\Gamma - M$ ($\Gamma - K$) for example, the TO modes split into $\Gamma - M_1$ and $\Gamma - M_2$ ($\Gamma - K_1$ and $\Gamma - K_2$) with the same trend as uniform strain circumstance by slopes of -40 cm^{-1}/% and -15.5 cm^{-1}/%, respectively. IR spectra resulting from biaxial strain are the sum of these two shifts (slope -55.5 cm^{-1}/%). The strain extracted from experimental spectra is presented in Figure 4d. In addition, we also obtained an analytical result of the strain distribution (black curve in Figure 4d) in the frame of materials elasticity (see Supporting Information Section 2), which matches quite well with the experimental result in the region that is ~500 nm away from strain center. A notable discrepancy, however, shows up close to the strain center, which is probably induced by the abnormal structure of the wrinkle (see Supporting Information Section 5). In our analytical calculation, we assume the winkle has a perfect folded structure, which will result in an infinite strain magnitude and a diverged strain energy density at its terminal. In reality, such a structure is energetically unstable, and the material would prefer to alter its local structure to lower the strain.

We briefly estimate the minimum strain that is detectable with s-SNOM, i.e. the

sensitivity of this technique. The strain is detectable only when the strain induced change of IR signal is greater than the noise level. On the one hand, the typical value of noise in our infrared images is ~2.5%. On the other hand, the largest slope of the spectral lines in Figure 4b is ~5%/cm^{-1} (see Supporting Information Section 6). Therefore, a frequency shift of 0.5 cm^{-1} is the minimum detectable frequency shift. Considering the strain induced frequency shift slope is ~50 cm^{-1}/%, we obtain the minimum strain that can be detected to be 0.01%, meaning that we are able to probe a relative lattice variation of 10^{-4} in hBN using this technique. The high sensitivity comes from strong near-field light-phonon coupling and high quality factor of the phonon resonance in hBN.

In conclusion, we have demonstrated phonon polariton assisted nanometer-scale mapping of local strain in atomically thin 2D polar crystal of hBN, which is based on the near-field infrared response close to the optical phonon frequency of hBN. We uncover that the infrared response has different origins for different frequency ranges: for frequencies lower than the TO phonon, it is determined by the local dielectric function; for frequencies higher than the TO phonon, it is affected by nonlocal phonon polaritons. The s-SNOM based local strain detection technique, with high sensitivity of being able to detect a strain as low as 10^{-4} in hBN, should work for a variety of low dimensional materials with polar crystal structures, such as bilayer graphene or MoS$_2$. The technique could be a complementary to TERS in the detection of phonon modes at the nanometer scale. In contrast to TERS which typically requires samples to be placed on metal substrates to enhance Raman signal, the introduced technique works for

Commented [H3]: Perhaps reference *ACS Photonics*, **2018**, *5* (7), pp 2773–2779

samples on various substrates. This technique could open up exciting opportunities to study local strain and local strain related physics in 2D materials and heterostructures on many substrates. In addition, the observed local strain induced phonon polariton reflection in hBN flakes could enable novel controlling of phonon polaritons at the nanometer scale for photonic devices.

Methods

Near-field IR imaging. A home-built IR-SNOM composed of a Bruker Innova AFM and a Daylight Solution quantum cascade laser (QCL) is used for the near-field IR imaging. A mid-infrared light (1340 – 1410 cm^{-1}) generated by the QCL laser was focused onto the apex of a conductive AFM tip. The enhanced optical field at the tip apex interacts with hBN underneath the tip. The scattered light, carrying local optical information of the sample, was collected by a MCT detector (KLD-0.1-J1, Kolmar) placed in the far field. Near-field optical images with spatial resolution better than 20 nm can be achieved with sharp AFM tips. Such near-field IR images are recorded simultaneously with the topography information during our measurements.

Nano-FTIR measurement. Approximately 500 µW of broadband synchrotron IR light from Beamline 5.4 at the Advanced Light Source (ALS) of Lawrence Berkeley National Laboratory is coupled to an asymmetric Michelson interferometer, consisting of a 50:50 KBr/Ge beamsplitter (Thermo-Scientific), a modified commercial AFM (Innova, Bruker), and a modified commercial FTIR spectrometer (Nicolet 6700, Thermo-Scientific). The beamsplitter directs half of the light to the scanning mirror in the FTIR

spectrometer and directs the other half to a parabolic mirror (N.A. ≈ 0.4) that focuses the beam onto an AFM tip. The backscattered light from the AFM tip, collected by the same parabolic mirror, and the light reflected from the moving mirror are recombined on the beamsplitter and focused onto an MCT detector (KLD-0.1-J1, Kolmar).

ASSOCIATED CONTENTS

Supporting Information

(1) Preparation of the strained hBN samples, (2) Theoretical estimation of the strain magnitude, (3) Local strain induced reflection of phonon polaritons, (4) First-principles calculations of strain induced phonon frequency shift in hBN, (5) Abnormal structure of the wrinkle, (6) Estimation of the sensitivity of the strain detection method.

AUTHOR INFORMATION

Corresponding Author

* Email: zwshi@sjtu.edu.cn (Z.S.)

Author contribution

Z.S. and B.L. conceived this project. B.L. prepared strained hBN samples and carried out near-field infrared strain measurements. H.L. derived analytical expression of the local strain. L.J., H.A.B., M.C.M. and F.W. carried out nano-FTIR measurement. W.S. performed first-principles phonon calculations under the supervision of W.L. C.H. performed COMSOL simulations. H.L., A.D., Z.Y., L.W. and Y.Z. helped with sample

preparation and optical measurements. All authors discussed the results and wrote the manuscript.

Notes

The authors declare no competing financial interest.

ABBREVIATIONS

2D, two dimensional; hBN, hexagonal boron nitride; SNOM, scanning near-field optical microscope; AFM, atomic force microscope; IR, infrared; TERS, tip-enhanced Raman spectroscopy; DFT, density functional theory.

REFERENCES

1.   Dean, C. R.; Young, A. F.; Meric, I.; Lee, C.; Wang, L.; Sorgenfrei, S.; Watanabe, K.; Taniguchi, T.; Kim, P.; Shepard, K. L.; Hone, J., Boron nitride substrates for high-quality graphene electronics. *Nature Nanotechnology* **2010,** *5*, 722.

2.   Wang, L.; Meric, I.; Huang, P. Y.; Gao, Q.; Gao, Y.; Tran, H.; Taniguchi, T.; Watanabe, K.; Campos, L. M.; Muller, D. A.; Guo, J.; Kim, P.; Hone, J.; Shepard, K. L.; Dean, C. R., One-Dimensional Electrical Contact to a Two-Dimensional Material. *Science* **2013,** *342* (6158), 614.

3.   Britnell, L.; Gorbachev, R. V.; Jalil, R.; Belle, B. D.; Schedin, F.; Mishchenko, A.; Georgiou, T.; Katsnelson, M. I.; Eaves, L.; Morozov, S. V.; Peres, N. M. R.; Leist, J.; Geim, A. K.; Novoselov, K. S.; Ponomarenko, L. A., Field-Effect Tunneling Transistor Based on Vertical Graphene Heterostructures. *Science* **2012,** *335* (6071), 947.

4.   Dean, C. R.; Wang, L.; Maher, P.; Forsythe, C.; Ghahari, F.; Gao, Y.; Katoch, J.; Ishigami, M.; Moon, P.; Koshino, M.; Taniguchi, T.; Watanabe, K.; Shepard, K. L.; Hone, J.; Kim, P., Hofstadter's butterfly and the fractal quantum Hall effect in moiré superlattices. *Nature* **2013,** *497*, 598.

5.   Chen, G.; Jiang, L.; Wu, S.; Lv, B.; Li, H.; Watanabe, K.; Taniguchi, T.; Shi, Z.; Zhang, Y.; Wang, F., Gate-Tunable Mott Insulator in Trilayer Graphene-Boron Nitride Moiré Superlattice. *arXiv preprint arXiv:1803.01985* **2018**.

6.   Yang, W.; Chen, G.; Shi, Z.; Liu, C.-C.; Zhang, L.; Xie, G.; Cheng, M.; Wang, D.; Yang, R.; Shi, D.; Watanabe, K.; Taniguchi, T.; Yao, Y.; Zhang, Y.; Zhang, G., Epitaxial growth of single-domain graphene on hexagonal boron nitride. *Nature Materials* **2013,** *12* (9), 792-797.

7.   Shi, Z.; Jin, C.; al., e., Gate-dependent pseudospin mixing in graphene/boron nitride moiré superlattices. *Nature Physics* **2014,** *10*.

8.   Hunt, B.; Sanchez-Yamagishi, J. D.; Young, A. F.; Yankowitz, M.; LeRoy, B. J.; Watanabe, K.; Taniguchi, T.; Moon, P.; Koshino, M.; Jarillo-Herrero, P.; Ashoori, R. C., Massive Dirac Fermions and Hofstadter Butterfly in a van der Waals Heterostructure. *Science* **2013,** *340* (6139), 1427.

9.   Dai, S.; Fei, Z.; Ma, Q.; Rodin, A. S.; Wagner, M.; McLeod, A. S.; Liu, M. K.; Gannett, W.; Regan, W.; Watanabe, K.; Taniguchi, T.; Thiemens, M.; Dominguez, G.; Neto, A. H. C.; Zettl, A.; Keilmann, F.; Jarillo-Herrero, P.; Fogler, M. M.; Basov, D. N., Tunable Phonon Polaritons in Atomically Thin van der Waals Crystals of Boron Nitride. *Science* **2014,** *343* (6175), 1125-1129.

10.   Shi, Z.; Bechtel, H. A.; Berweger, S.; Sun, Y.; Zeng, B.; Jin, C.; Chang, H.; Martin, M. C.; Raschke, M. B.; Wang, F., Amplitude- and Phase-Resolved Nanospectral Imaging of Phonon Polaritons in Hexagonal Boron Nitride. *ACS Photonics* **2015,** *2* (7), 790-796.

11.   Guinea, F.; Katsnelson, M. I.; Geim, A. K., Energy gaps and a zero-field quantum Hall effect in graphene by strain engineering. *Nat Phys* **2010,** *6* (1), 30-33.

12.   Pereira, V. M.; Castro Neto, A. H., Strain engineering of graphene's electronic structure. *Phys Rev Lett* **2009,** *103* (4), 046801.

13.   Levy, N.; Burke, S. A.; Meaker, K. L.; Panlasigui, M.; Zettl, A.; Guinea, F.; Neto, A. H. C.; Crommie, M. F., Strain-Induced Pseudo–Magnetic Fields Greater Than 300 Tesla in Graphene Nanobubbles. *Science* **2010,** *329* (5991), 544.

14.   Ju, L.; Shi, Z.; Nair, N.; Lv, Y.; Jin, C.; Velasco Jr, J.; Ojeda-Aristizabal, C.; Bechtel, H. A.; Martin, M. C.; Zettl, A.; Analytis, J.; Wang, F., Topological valley transport at bilayer graphene domain walls. *Nature* **2015,** *520*, 650.

15.   Jiang, L.; Shi, Z.; Zeng, B.; Wang, S.; Kang, J.-H.; Joshi, T.; Jin, C.; Ju, L.; Kim, J.; Lyu, T.; Shen, Y.-R.; Crommie, M.; Gao, H.-J.; Wang, F., Soliton-dependent plasmon reflection at bilayer graphene domain walls. *Nature Materials* **2016,** *15*, 840.

16.   Castellanos-Gomez, A.; Roldan, R.; Cappelluti, E.; Buscema, M.; Guinea, F.; van der Zant, H. S.; Steele, G. A., Local strain engineering in atomically thin MoS2. *Nano Lett* **2013,** *13* (11), 5361-6.

17.   Ji, C.; Levitas, V. I.; Zhu, H.; Chaudhuri, J.; Marathe, A.; Ma, Y., Shear-induced phase transition of nanocrystalline hexagonal boron nitride to wurtzitic structure at room temperature and lower pressure. *Proc Natl Acad Sci U S A* **2012,** *109* (47), 19108-12.

18.   Di Fonzo, S.; Jark, W.; Lagomarsino, S.; Giannini, C.; De Caro, L.; Cedola, A.; Muller, M., Non-destructive determination of local strain with 100-nanometre spatial resolution. *Nature* **2000,** *403* (6770), 638-40.

19.   Wang, Y.-D.; Tian, H.; Stoica, A. D.; Wang, X.-L.; Liaw, P. K.; Richardson, J. W., The development of grain-orientation-dependent residual stressess in a cyclically deformed alloy. *Nature Materials* **2003,** *2*, 101.

20.   Hÿtch, M.; Houdellier, F.; Hüe, F.; Snoeck, E., Nanoscale holographic interferometry for strain measurements in electronic devices. *Nature* **2008,** *453,* 1086.

21.   Beams, R.; Cancado, L. G.; Jorio, A.; Vamivakas, A. N.; Novotny, L., Tip-enhanced Raman mapping of local strain in graphene. *Nanotechnology* **2015,** *26* (17), 175702.

22.   Yano, T.; Ichimura, T.; Kuwahara, S.; H'Dhili, F.; Uetsuki, K.; Okuno, Y.; Verma, P.; Kawata, S., Tip-enhanced nano-Raman analytical imaging of locally induced strain distribution in carbon nanotubes. *Nature Communications* **2013,** *4*.

23.   Fei, Z.; Rodin, A. S.; Andreev, G. O.; Bao, W.; McLeod, A. S.; Wagner, M.; Zhang, L. M.; Zhao, Z.; Thiemens, M.; Dominguez, G.; Fogler, M. M.; Neto, A. H. C.; Lau, C. N.; Keilmann, F.; Basov, D. N., Gate-tuning of graphene plasmons revealed by infrared nano-imaging. *Nature* **2012,** *487*, 82.

24.   Lundeberg, M. B.; Gao, Y.; Asgari, R.; Tan, C.; Van Duppen, B.; Autore, M.; Alonso-Gonzalez, P.; Woessner, A.; Watanabe, K.; Taniguchi, T.; Hillenbrand, R.; Hone, J.; Polini, M.; Koppens, F. H. L., Tuning quantum nonlocal effects in graphene plasmonics. *Science* **2017,** *357* (6347), 187-191.

25.   Shi, Z.; Hong, X.; Bechtel, H. A.; Zeng, B.; Martin, M. C.; Watanabe, K.; Taniguchi, T.; Shen, Y.-R.; Wang, F., Observation of a Luttinger-liquid plasmon in metallic single-walled carbon nanotubes. *Nature Photonics* **2015,** *9*, 515.

26.   Ni, G. X.; McLeod, A. S.; Sun, Z.; Wang, L.; Xiong, L.; Post, K. W.; Sunku, S. S.; Jiang, B. Y.; Hone, J.; Dean, C. R.; Fogler, M. M.; Basov, D. N., Fundamental limits to graphene plasmonics. *Nature* **2018,** *557* (7706), 530-533.

27.   Huber, A. J.; Ziegler, A.; Kock, T.; Hillenbrand, R., Infrared nanoscopy of strained semiconductors. *Nat Nanotechnol* **2009,** *4* (3), 153-7.

28.   Gigler, A. M.; Huber, A. J.; Bauer, M.; Ziegler, A.; Hillenbrand, R.; Stark, R. W., Nanoscale residual stress-field mapping around nanoindents in SiC by IR s-SNOM and confocal Raman microscopy. *Opt. Express* **2009,** *17* (25), 22351-22357.

29.   Bensmann, S.; Gaußmann, F.; Lewin, M.; Wüppen, J.; Nyga, S.; Janzen, C.; Jungbluth, B.; Taubner, T., Near-field imaging and spectroscopy of locally strained GaN using an IR broadband laser. *Opt. Express* **2014,** *22* (19), 22369-22381.

30.   Liu, M.; Sternbach, A. J.; Wagner, M.; Slusar, T. V.; Kong, T.; Bud'ko, S. L.; Kittiwatanakul, S.; Qazilbash, M. M.; McLeod, A.; Fei, Z.; Abreu, E.; Zhang, J.; Goldflam, M.; Dai, S.; Ni, G.-X.; Lu, J.; Bechtel, H. A.; Martin, M. C.; Raschke, M. B.; Averitt, R. D.; Wolf, S. A.; Kim, H.-T.; Canfield, P. C.; Basov, D. N.,

Phase transition in bulk single crystals and thin films of VO2 by nanoscale infrared spectroscopy and imaging. *Physical Review B* **2015,** *91* (24), 245155.

31.   Oliveira, C. K.; Gomes, E. F. A.; Prado, M. C.; Alencar, T. V.; Nascimento, R.; Malard, L. M.; Batista, R. J. C.; de Oliveira, A. B.; Chacham, H.; de Paula, A. M.; Neves, B. R. A., Crystal-oriented wrinkles with origami-type junctions in few-layer hexagonal boron nitride. *Nano Research* **2015,** *8* (5), 1680-1688.

32.   Bechtel, H. A.; Muller, E. A.; Olmon, R. L.; Martin, M. C.; Raschke, M. B., Ultrabroadband infrared nanospectroscopic imaging. *Proceedings of the National Academy of Sciences* **2014,** *111* (20), 7191.

Table of Contents Graphic